Validation of mass-market GNSS and IMU MEMS sensors for millimeter-level displacement retrieval under simulated vibrations

Jacek PAZIEWSKI[1,*], **Rafal SIERADZKI**[1], **Jakub KOSCIELSKI**[1], **Hubert SZCZEPANIK**[1], **Dariusz TOMASZEWSKI**[1], and **Katarzyna STEPNIAK**[1]

[1] *University of Warmia and Mazury in Olsztyn, Olsztyn, Poland, (jacek.paziewski@uwm.edu.pl, rafal.sieradzki@uwm.edu.pl, jakub.koscielski@student.uwm.edu.pl, hubert.szczepanik@student.uwm.edu.pl, dariusz.tomaszewski@uwm.edu.pl, katarzyna.stepniak@uwm.edu.pl)*

[*] *corresponding author*

Abstract

In this study, we validate selected low-cost GNSS receivers, namely u-blox ZED-F9P, and Septentrio Mosaic-X5, and their fusion with RedShift Labs UM7 MEMS sensor for millimeter-level displacement retrieval. The observation assessment reveals that low-cost GNSS data's accuracy is competitive with high-grade receivers. Furthermore, in the case of Septentrio Mosaic-X5 GNSS, we note the outperformance of its code measurements over those of the high-grade receiver. Next, we assess the performance of the low-cost GNSS-PPP and coupled low-cost GNSS & MEMS accelerometer high-rate solutions under vibrations simulated with a shake table. The high performance of both solutions based on low-cost sensors is confirmed. We report an advantage of the coupled solution over the GNSS-only one documented with a meaningful reduction of the displacement error. With a coupled solution of mass-market sensors, we prove the feasibility of detecting the vibration even of 1 mm amplitude. The time-frequency analyses also indicate that both coupled and single-sensor solutions may successfully detect the vibration frequencies; however, they also confirm the outperformance of the former over the latter. Coupled solutions are less noisy for the high-frequency band than the GNSS-only one.

Keywords: low-cost GNSS, dynamic displacement, high-rate GNSS, structural health monitoring, MEMS IMU, vibrations

1 Introduction

Recently, we have noted progress in low-cost GNSS receivers that led to their performance being close to that of high-grade instruments. Consequently, the capabilities of low-cost GNSS receivers complemented with other sensors, e.g., IMU, induce an increased interest in their application to structural health monitoring (SHM) and seismogeodesy. Conventionally, such demanding applications as SHM or seismic studies were conducted with sole high-grade seismometer/accelerometer sensors. With the past progress in GNSS signal acquisition hardware and processing methods, GNSS is now considered a mature technique that addresses the requirements of such precise applications (Lovse et al., 1995). Numerous studies have proved the high applicability of high-grade GNSS receivers to SHM or seismogeodesy (Colosimo et al., 2011; Yigit et al., 2017; Hohensinn et al., 2020). The most essential advantages of GNSS are the feasibility of providing absolute position changes and both vibrations and deformation solutions (Im et al., 2013). Nonetheless, the application of typical GNSS receivers has its limitations, such as low in relation to seismometers, sampling rate, non-negligible temporal correlation of observations, phase lock loop-induced effects, and high cost of purchase (Paziewski et al., 2020). Also, the sole application of professional seismometers results in outcomes burdened by tilt, rotation, and hysteresis, which consequently produces the displacement of the relative nature (Allen et al., 2003). An integration of GNSS and accelerometer may address the aforementioned constraints.

Moreover, the advent of mass-market low-cost GNSS chipsets/receivers and Micro-Electro-Mechanical Systems (MEMS) Inertial Measurement Units (IMU) and Attitude and Heading Reference Systems (AHRS) motivated us to combine such sensors for the precise detection of dynamic vibrations, at a millimeter level. In this study, we verify a research hypothesis of whether integrated solutions of non-professional mass-market GNSS and accelerometer MEMS sensors may detect dynamic displacements with millimeter-level precision. For this purpose, we have conducted an experiment to retrieve the vibrations induced by the shake table and provide reliable benchmark results.

2 Methods

To retrieve the simulated vibrations, we loosely integrated GNSS and accelerations from IMU MEMS sensors. Such an approach assumes prior determination of displacements through the temporal difference of coordinates derived from high-rate (HR) GNSS solution. In this step, we employed a high-rate precise point positioning technique (HR-PPP). The PPP decoupled-clock model (DCM) based on uncombined dual-frequency GPS observations (Teunissen et al., 2015) was implemented in own-developed software and employed to process high-rate data. The DCM model takes advantage of ambiguity datum to handle the rank deficiency of the observation system. All the conventional correction models (antenna phase center corrections, phase wind-up, pseudorange biases, etc.) together with the precise orbits and clocks from CNES to retrieve uncombined phase delays were employed to provide the feasibility of a PPP solution with integer ambiguity resolution (PPP-AR/PPP-RTK). However, due to the extremely short data acquisition period and lack of precise external ionospheric corrections, we did not persuade the ambiguities fixing; thus, float solutions were also accepted, as the final GNSS PPP solution was subject to high-pass Butterworth filtering (Butterworth, 1930).

Next, the PPP-derived displacements are combined with the acceleration records according to the algorithm (Paziewski et al., 2025). The state-space model (x) includes two state variables, namely displacements (d) and velocities (v) at epoch (i):

$$x_i = [d_i \quad v_i]^T \tag{1}$$

in the dynamical system model, which is given as follows:

$$x_{i+1} = Ax_i + Bu_i + w_i \tag{2}$$

with u representing a vector of the accelerations acquired by the MEMS sensor, w denoting the vector of the system noise, A referring to the system state transition matrix, and B indicating the input matrix.

The measurement model of GNSS-derived displacements (z) is then given as below:

$$z_i = Hx_i + \nu_i \tag{3}$$

where H stands for the design matrix, which shows the linkage between the measurement and state vectors, and ν refers to the vector describing GNSS displacement noise.

Such integration is conventionally executed with the Kalman filter (Grewal et al., 2015), as both GNSS and accelerometer data are provided with a different sampling rate (Bock et al., 2011). Finally, the backward filtering with the Rauch Tung Striebel algorithm is performed (Rauch et al., 1965).

3 Experiment design

We simulated artificial single-direction horizontal low-scale vibrations, which we aimed to retrieve based on GNSS & accelerometer data processing. A Quanser I-40 single-axis shake table was used to induce five harmonic motions of 1 Hz frequency and amplitudes from 20 to 1 mm (Table 1).

Table 1. Parameters of the vibrations simulated in the experiment with the shake table.

# of vibration	**Amplitude [mm]**	**Frequency [Hz]**
1	20	1
2	10	1
3	5	1
4	2.5	1
5	1	1

On the shake table platform, we have mounted RedShift Labs UM7 AHRS MEMS sensor and Septentrio PolaNt* MC.v2 antenna, to which, with a splitter, three GNSS receivers were connected to record observations. We used two low-cost GNSS receivers, namely Septentrio Mosaic X5 and u-blox ZED F9P, operating with a 10 Hz data sampling rate for GNSS data acquisition. As a benchmark receiver, we employed high-grade Trimble Alloy, which was set to acquire GNSS data at the same rate.

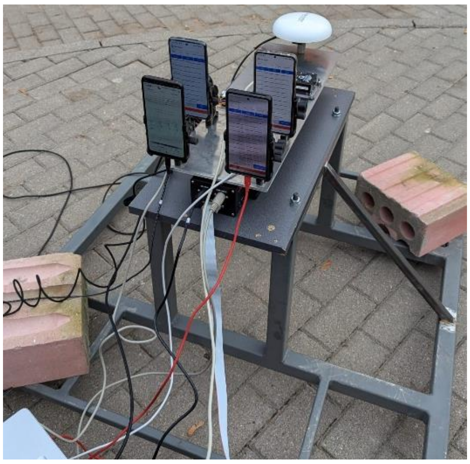

Figure 1. A set-up used for data acquisition, which consists of Quanser I-40 shake table, low-cost and high-grade receivers acquiring signals from Septentrio PolaNt* MC.v2 antenna, and RedShift Labs UM7 AHRS MEMS sensors.

With the algorithms presented in Sect. 2, we have integrated accelerometer records of 50 Hz and GNSS PPP-derived high-rate displacements of 10 Hz. We have validated both GNSS-only and integrated GNSS & accelerometer solutions in terms of harmonic motion parameters against the benchmark sets of the simulation scenario (Table 1).

4 Results

We precede validating the solution provided by the fusion of GNSS & accelerometer with the sensor data assessment. In this regard, we assess the HR-GNSS data provided by all the analyzed sensors regarding phase and code noise and stochastic characteristics of the accelerations recorded by the RedShift Labs UM7 AHRS MEMS sensor.

4.1 Low-cost GNSS and MEMS accelerometer data assessment

We analyze the quality of GNSS phase data, being a key factor driving the accuracy of the PPP solution. For this purpose, we used zero- and short-baseline (1.6 m) experiments built of homogeneous pairs of the low-cost receivers (Septentrio Mosaic-X5 and u-blox ZED-F9P) and the set of Trimble Alloy instruments serving as a benchmark. The tests were conducted in an unobstructed sky view. The double-differenced (DD) data time series for the selected arcs of GPS satellites were detrended with third-order polynomials to eliminate the ambiguity terms and slow changes of satellite geometry (only the short-baseline scenario). Finally, we computed the standard deviation (STD) of such time series for particular receivers (Table 2).

Table 2. Phase noise levels for different scenarios and instruments.

STD of DD GPS phase residuals [mm]						
	Trimble		**Sept.**		**u-blox**	
	L1	**L2**	**L1**	**L2**	**L1**	**L2**
Zero-bas.	1.2	1.4	0.6	1.0	1.0	1.3
Short-bas.	3.9	5.8	3.2	5.0	3.8	6.0

The results for the zero-baseline, depicting the levels of thermal noise, reveal the superiority of Septentrio Mosaic-X5. Also, the statistics for the u-blox ZED-F9P are slightly better than for the Trimble Alloy. This unexpectedly high quality of the low-cost data is believed to be driven by the receiver settings. According to our preliminary analysis in a frequency domain, the power spectrum for Trimble Alloy is almost flat, corresponding to white noise. In contrast, the high-frequency components for the low-cost receivers are approximately an order of magnitude lower, which explains the better statistics in the latter case. This high-frequency noise reduction also propagates to results for the short-baseline scenario, where the obtained deviation corresponds to a sum of thermal noise and phase multipath. While the comparison of results for both tests indicates that the latter factor has a dominant role, the difference of STD for Septentrio Mosaic-X5 and Trimble Alloy is similar. Thus, we find the multipath impact for both receivers to be comparable. The results for u-blox ZED-F9P are slightly more degraded for the short-baseline scenario but still should be considered a good quality.

For IMU sensors, random walk is typically used to quantify the randomness associated with inertial sensors. It represents the direct influence of uncorrelated noise on computed velocities in accelerometers. This phenomenon arises from integrating white noise from inertial sensors, leading to a standard deviation that increases proportionally to the square root of time. In the case of accelerometer readings, this phenomenon is called velocity random walk (VRW). A method that is most commonly used for estimating the value of VRW is the Allan Variance (AV). AV analysis was fed with the RSX data collected for 72 hours. The AV analysis in Figure 2 confirmed that the RSX module can be considered a suitable component for precise vibration monitoring.

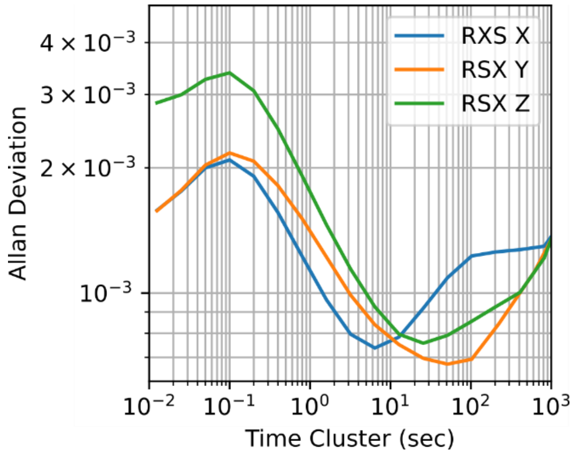

Figure 2. Allan Variance graph for leveled RSX IMU accelerometer.

4.2 Assessment of the vibration retrieval

In Figure 3, we show an example of a displacement time series retrieved from GNSS-only and integrated GNSS & accelerometer solutions. The figure clearly shows how the GNSS-only solution may provide overestimated amplitudes. However, such an effect is not observed for the accelerometer-only and combined GNSS+Acc solutions.

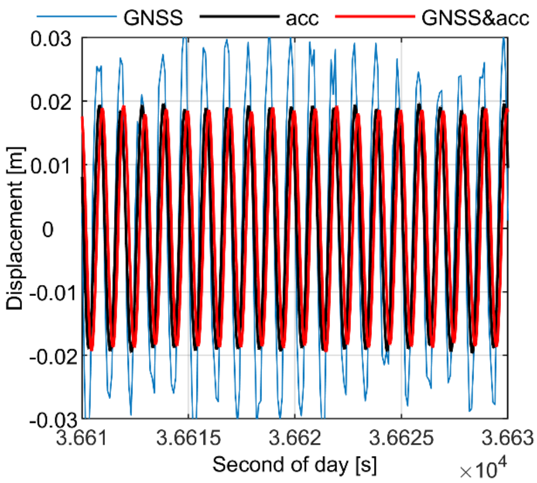

Figure 3. Time series of retrieved displacements during harmonic motion #1 of 20 mm amplitude for GNSS-PPP-only (GNSS), accelerometer-only (acc), and integrated GNSS & accelerometer (GNSS&acc) solutions with Trimble Alloy receiver.

Figure 4 presents the example results of the Fast Fourier Transform (FFT) for the displacement time series retrieved during simulated excitation #1 of 10 mm amplitude and 1 Hz frequency. Again, the results confirm the overestimation of the GNSS-only derived displacements. On the contrary, the integrated solution is not subject to such undesired effects.

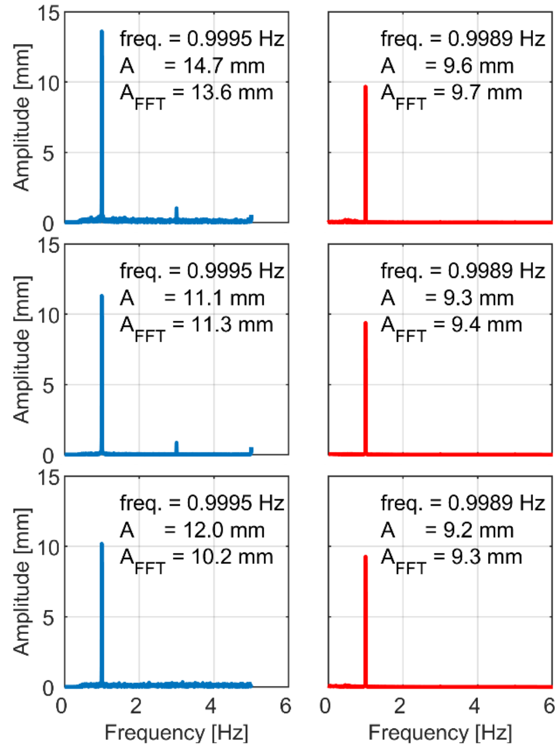

Figure 4. FFT spectra for excitation #1 (10 mm amp., 1 Hz freq.) for GNSS-only solution (left) and GNSS+Acc. (right) with Trimble, Septentrio, and u-blox in the top, middle, and bottom panels.

The results of retrieved amplitudes for GNSS-PPP-only and integrated GNSS & accelerometer solutions are given in Table 3. We show the benchmark (simulated) amplitude and the true error of the mean amplitude retrieved from the displacement time series.

Table 3. Amplitude (A) true errors as a difference between the benchmark and the amplitude retrieved from the GNSS-PPP-only (GNSS) and the integrated (GNSS+acc) solutions.

		Amplitude error [mm]					
		Trimble		Sept.		u-blox	
#	A [mm]	GNSS	GNSS +acc	GNSS	GNSS +acc	GNSS	GNSS +acc
1	20	8.9	-1.4	3.6	-1.6	1.8	-1.9
2	10	4.7	-0.4	1.1	-0.7	2.0	-0.7
3	5	3.5	-0.5	1.1	-0.5	1.8	0.6
4	2.5	3.3	-0.3	0.3	-0.3	0.3	-0.3
5	1	3.6	-0.2	0.4	-0.2	3.3	-0.2

Considering the GNSS-PPP solutions, we may conclude that the Trimble Alloy receiver provided the displacements of the lowest accuracy, as the errors of the retrieved amplitudes were the highest, between 3.3 and 8.9 mm. The retrieved amplitudes for this receiver consistently exceed the simulated ones. This aligns with the example displacement time series, as they also exhibit overestimation. For the low-cost receivers, the amplitude errors were mostly below 2 mm. Again, the low-cost GNSS-only solution always provided slightly magnified amplitudes with regard to the benchmark values. After the integration of the GNSS-PPP solution with the MEMS acceleration records, the errors have dropped significantly. In the case of excitations #2-5 with the designed amplitudes of 10–1 mm, the errors of the retrieved amplitude have not exceeded 0.7 mm. Even the vibrations of 1 mm (#5) could be reliably detected with the error of 0.2 mm.

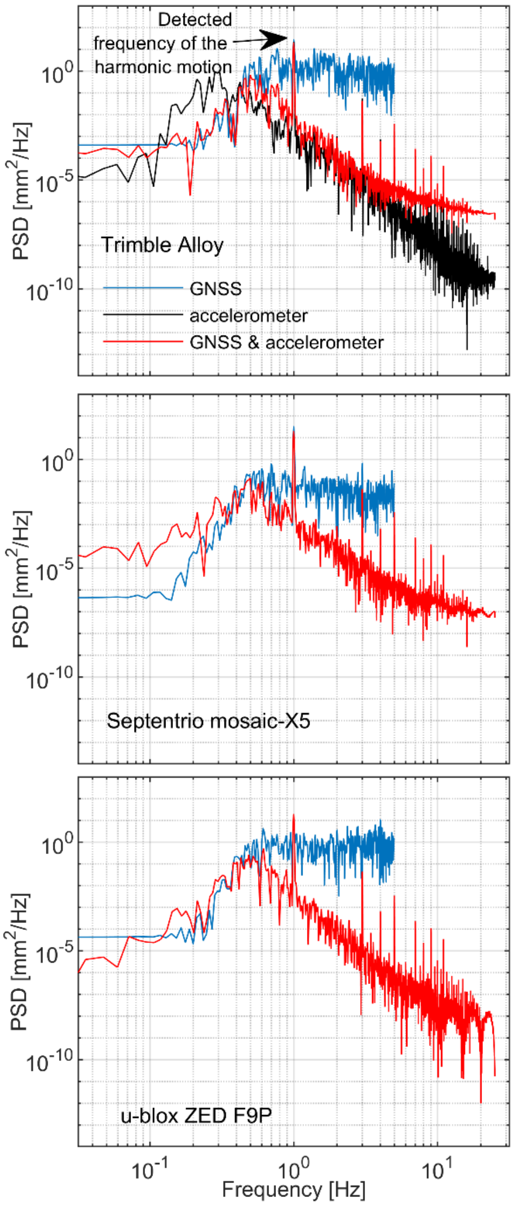

Figure 5. PSD for displacement time series during excitation #5 of 1 mm amplitude and 1 Hz frequency for GNSS-only and integrated solutions. The black line corresponds to the displacements double integrated from the accelerometer readings.

Figure 5 shows Welch's power spectral density (PSD) of the vibrations retrieved with GNSS-only, accelerometer-only, and integrated solutions under the most challenging excitations of 1 mm amplitude. The results tell us how including the accelerometer records reduces the noise in the coupled solution compared to GNSS-only, for high-frequency bands (> 1 Hz).

5 Conclusions

We verified the research hypothesis on the feasibility of recovering mm-level dynamic displacements with the integrated low-cost GNSS and MEMS accelerometer sensors. In the experiment, we used u-blox ZED-F9P and Septentrio Mosaic-X5 and fused them with RedShift Labs UM7 MEMS sensor as observation acquisition devices. The low-scale vibrations of the amplitude between 20 and 1 mm were induced with Quanser I-40 shake. A high-grade GNSS receiver - Trimble Alloy, was used as a benchmark receiver for GNSS data assessment and high-rate GNSS solution provider.

The observation assessment revealed that low-cost GNSS data's accuracy is competitive with high-grade receivers. More specifically, in the case of Septentrio Mosaic-X5 GNSS, we note the outperformance of its phase measurements over those of the high-grade receiver.

Next, we assessed the performance of the low-cost GNSS-only and coupled GNSS & MEMS accelerometer high-rate solutions under vibrations simulated with a shake table. We report an advantage of the coupled solution over the GNSS-only one documented with a meaningful reduction of the displacement error. After the integration of the GNSS-PPP solution with the MEMS acceleration records, mostly the errors of the retrieved amplitudes did not exceed 0.7 mm, and even the vibrations of 1 mm amplitude could be reliably detected, as the amplitude errors equaled 0.2 mm. The GNSS-only solution, in turn, always provided overestimated amplitudes. The time-frequency analyses also indicated that both coupled and single-sensor solutions may successfully detect the vibration frequencies; however, they also confirm the outperformance of the former over the latter. Coupled solutions are less noisy for the high-frequency band than the GNSS-only one.

Acknowledgements

This research was funded in whole or in part by the National Science Centre, Poland Project No. 2023/48/Q/ST10/00059. For the purpose of Open Access, the author has applied a CC-BY public copyright licence to any Author Accepted Manuscript (AAM) version arising from this submission.

References

Allen, R. M., & Kanamori, H. (2003). The Potential for Earthquake Early Warning in Southern California. *Science*, *300*(5620), 786–789. doi: 10.1126/science.1080912

Bock, Y., Melgar, D., & Crowell, B. W. (2011). Real-Time Strong-Motion Broadband Displacements from Collocated GPS and Accelerometers. *Bulletin of the Seismological Society of America*, *101*(6), 2904–2925. doi: 10.1785/0120110007

Butterworth, S. (1930). On the Theory of Filter Amplifiers. *Experimental Wireless & the Wireless Engineer*, *7*, 536–541.

Colosimo, G., Crespi, M., & Mazzoni, A. (2011). Real-time GPS seismology with a stand-alone receiver: A preliminary feasibility demonstration. *Journal of Geophysical Research: Solid Earth*, *116*(B11), B11302. doi: 10.1029/2010JB007941

Grewal, M. S., & Andrews, A. P. (2015). *Kalman filtering: theory and practice using MATLAB* (Fourth edition). Hoboken, New Jersey: John Wiley & Sons Inc.

Hohensinn, R., Häberling, S., & Geiger, A. (2020). Dynamic displacements from high-rate GNSS: Error modeling and vibration detection. *Measurement*, *157*, 107655. doi: 10.1016/j.measurement.2020.107655

Im, S. B., Hurlebaus, S., & Kang, Y. J. (2013). Summary Review of GPS Technology for Structural Health Monitoring. *Journal of Structural Engineering*, *139*(10), 1653–1664. doi: 10.1061/(ASCE)ST.1943-541X.0000475

Lovse, J. W., Teskey, W. F., Lachapelle, G., & Cannon, M. E. (1995). Dynamic Deformation Monitoring of Tall Structure Using GPS Technology. *Journal of Surveying Engineering*, *121*(1), 35–40. doi: 10.1061/(ASCE)0733-9453(1995)121:1(35)

Paziewski, J., Kurpinski, G., Wielgosz, P., Stolecki, L., Sieradzki, R., Seta, M., Oszczak, S., Castillo, M., & Martin-Porqueras, F. (2020). Towards Galileo + GPS seismology: Validation of high-rate GNSS-based system for seismic events characterisation. *Measurement*, *166*, 108236. doi: 10.1016/j.measurement.2020.108236

Paziewski, J., Sieradzki, R., Rapinski, J., Tomaszewski, D., Stepniak, K., Geng, J., & Li, G. (2025). Integrating low-cost GNSS and MEMS accelerometer for precise dynamic displacement monitoring. *Measurement*, *242*, 115798. doi: 10.1016/j.measurement.2024.115798

Rauch, H. E., Tung, F., & Striebel, C. T. (1965). Maximum likelihood estimates of linear dynamic systems. *AIAA Journal*, *3*(8), 1445–1450. doi: 10.2514/3.3166

Teunissen, P. J. G., & Khodabandeh, A. (2015). Review and principles of PPP-RTK methods. *Journal of Geodesy*, *89*(3), 217–240. doi: 10.1007/s00190-014-0771-3

Yigit, C. O., & Gurlek, E. (2017). Experimental testing of high-rate GNSS precise point positioning (PPP) method for detecting dynamic vertical displacement response of engineering structures. *Geomatics, Natural Hazards and Risk*, *8*(2), 893–904.